Hybrid Living Materials: Digital Design and Fabrication of 3D Multimaterial Structures with Programmable Biohybrid Surfaces

Rachel Soo Hoo Smith, Christoph Bader, Sunanda Sharma, Dominik Kolb, Tzu-Chieh Tang, Ahmed Hosny, Felix Moser, James C. Weaver, Christopher A. Voigt, and Neri Oxman*

Significant efforts exist to develop living/non-living composite materials—known as biohybrids—that can support and control the functionality of biological agents. To enable the production of broadly applicable biohybrid materials, new tools are required to improve replicability, scalability, and control. Here, the Hybrid Living Material (HLM) fabrication platform is presented, which integrates computational design, additive manufacturing, and synthetic biology to achieve replicable fabrication and control of biohybrids. The approach involves modification of multimaterial 3D-printer descriptions to control the distribution of chemical signals within printed objects, and subsequent addition of hydrogel to object surfaces to immobilize engineered *Escherichia coli* and facilitate material-driven chemical signaling. As a result, the platform demonstrates predictable, repeatable spatial control of protein expression across the surfaces of 3D-printed objects. Custom-developed orthogonal signaling resins and gene circuits enable multiplexed expression patterns. The platform also demonstrates a computational model of interaction between digitally controlled material distribution and genetic regulatory responses across 3D surfaces, providing a digital tool for HLM design and validation. Thus, the HLM approach produces biohybrid materials of wearable-scale, self-supporting 3D structure, and programmable biological surfaces that are replicable and customizable, thereby unlocking paths to apply industrial modeling and fabrication methods toward the design of living materials.

1. Introduction

Living cells host a diverse and extensive repertoire of processes that, if functionalized, would have extraordinary value as synthetic tools.[1–4] Yet, beyond the confines of industrial bioreactors, there are limited examples of how bioengineers can utilize the functionalities of living cells reliably, at macroscopic length scales, or outside of cells' natural environments. At present, the field of biohybrid materials combines living and nonliving components with the objective of harnessing the capabilities of biological systems within structural materials.[5] Living cells integrated into biohybrid walls,[6–9] biohybrid fibers,[10–12] and bio-bots[13–16] provide early examples of how such fabrications can enable a new class of uniquely responsive and multifunctional products. However, for biohybrid materials to be employed in similar manners as their industrial material counterparts, which can produce consistent outcomes on-demand, new tools must be developed to solve problems related to replicability, scalability, and standardized control. In this paper, we introduce Hybrid Living Materials (HLMs) as a subfield that aims to interface genetic engineering with material fabrication platforms to expand the ways in which living cells can be functionalized to generate new material properties, while also solving the shortcomings of controllability found in existing biohybrid materials.

Existing approaches for biohybrid control largely originate in techniques found in rapid fabrication, tissue engineering, and implantable or drug-eluting biomaterials. Examples include the direct printing of cells (i.e., bioprinting),[17,18] seeding cells into scaffolds or media,[19–21] and engineering cells to endogenously grow the structural materials that they inhabit.[22–24] Further, many of these examples have leveraged "digital fabrication"—the translation of digital designs into physical form with the precise and replicable control of computer-aided design (CAD) and manufacturing (CAM). Additive manufacturing platforms that directly place bio-inks (e.g., build material consisting of whole cell suspensions) into controlled shapes have emerged as a prevailing digital fabrication-driven biohybrid

R. S. H. Smith, C. Bader, S. Sharma, D. Kolb, T.-C. Tang, Prof. N. Oxman
MIT Media Lab
Massachusetts Institute of Technology
Cambridge, MA 02139, USA
E-mail: neri@mit.edu
T.-C. Tang, Dr. F. Moser, Prof. C. A. Voigt
Department of Biological Engineering
Synthetic Biology Center
Massachusetts Institute of Technology
Cambridge, MA 02139, USA
A. Hosny
Dana-Farber Cancer Institute
Harvard Medical School
Boston, MA 02115, USA
Dr. J. C. Weaver
Wyss Institute for Biologically Inspired Engineering
Harvard University
Cambridge, MA 02138, USA

**ADVANCED
SCIENCE NEWS**
www.advancedsciencenews.com

**ADVANCED
FUNCTIONAL
MATERIALS**
www.afm-journal.de

approach.[25–28] Digital fabrication platforms have also been used to template exogenous chemical or environmental signals. This targeted stimuli approach takes advantage of the sensing functions of individual cells to control specific cellular functions (e.g., protein expression) and multicellular behaviors (e.g., producing predefined patterns), for example, on the basis of light signals[29,30] or chemical signals laid down by a 2D inkjet printer.[31] Importantly, a few examples of this stimuli-driven technique have further harnessed synthetic biology in bacterial cells, thereby simultaneously designing for and controlling both internal biological functions and external stimuli. These approaches include regulating gene expression in bacterial cells to exhibit "edge detection" and other pattern formations.[32]

Here we present an HLM fabrication platform and a supporting computer-aided design tool that unify the control of form, material, and cellular response during the creation of macroscale hybrid living objects. In this methodology, we take existing tools from the computational design and digital fabrication fields that are used to control volumetric material distributions for 3D inkjet printing[33,34] and translate them into tools for the programmable control of biological behavior across the surface of 3D-printed objects. To interface a multimaterial inkjet-based 3D printer with cellular functionality, we employ two well-developed biomaterial regimes: the use of diffusive chemicals for cell signaling[35–37] and the use of hydrogel environments to immobilize cells across the surface of 3D structures.[25,38,39] Unlike prior approaches, the HLM platform uses a holistic design-to-fabrication workflow to digitally model and control the gene-regulated function of engineered bacteria in response to targeted chemical signals programmed into the 3D object. The resulting outputs can be human-scale objects with programmable biological surfaces which are customized, replicable, and made on-demand.

To address challenges of controllability and design ability facing the biohybrid field, this work establishes a scaled, replicable system for controlling and modeling the gene-regulated function of engineered bacteria in response to chemical signals on a 3D-material surface. The "Experimental Section" describes the HLM digital fabrication platform, detailing a chemical templating strategy developed by exploiting digital commands on a commercial multimaterial printer to produce unique print material blends that interface with hydrogel properties. The "Results" section addresses the feasibility of using digital material descriptions to guide bacterial gene expression across the surface of 3D-printed objects. First, we characterized the repeatability and spatial regulation that printed material distributions allowed for the tunable release of chemical signals and induction of protein expression. We demonstrated a diversity of complex, freestanding geometries, varying mechanical rigidities (flexible, elastic, and soft), and different opacities available to HLM constructs. Second, we showed that chemical augmentation of the printer resins enabled deposition of multiple chemical signal channels during the 3D-printing process. This feature enabled HLMs with synthetic regulatory circuits (i.e., multi-input pattern drivers) to produce multiplexed and logic-based expression patterns. Finally, we established a computational model for chemical diffusion dynamics and biological response across arbitrary 3D surfaces that is applicable to the CAD environment in which HLMs are designed. In summary, the HLM platform provides

a new tool for designers, engineers, and scientists to program custom, tractable expression into biohybrid constructs, and thus control engineered bacterial functionalities with digital material technology across a broad range of applications.

2. Experimental Section

2.1. Platform Overview

The platform overview presents the integrated framework for the controlled fabrication of HLMs, comprising computational design, digital fabrication, and genetic engineering techniques (**Figure 1**). The biohybrid face mask featured in this example was digitally modeled to custom fit a human face and produce a prescribed biological response (i.e., colored patterning indicating locally tunable gene-regulated protein expression), demonstrating a potential use as a delivery system for topical therapies relating to site-specific and custom facial devices[40–43] and bacterial therapies.[44–47]

In this process, the planning of HLM objects began in a computer-aided design environment (Figure 1a–c). A "volumetric material description" represents a 3D object as a set of voxels (3D pixels) arranged in a regular grid. Unlike stereolithographic (STL) file formats, which assign one material per mesh-bounded object,[33] voxel-based descriptions assign a specific material composition to each voxel to represent both an overall geometry of an object (Figure 1a) and a heterogeneous distribution of materials throughout its volume (Figure 1b). In this method, digital modeling tools were extended, first, to designate how chemical signals are distributed in the object, and second, to estimate the biological response in relation to the geometry and concentration of signal in the object (Figure 1c).

The digital object file was next prepared for digital fabrication on a photopolymeric inkjet-based 3D printer (Figure 1d–f). A "digital material" is defined here as a mixing ratio of resins that the inkjets are able to combine "on-the-fly" during the printing process.[48] When a volumetric material description is translated to the print environment, the material composition of each voxel is decoded into droplets of different distinct materials. Given the arbitrary size of a voxel in relation to the droplet resolution of the printer, a single voxel may be decoded to several droplets (Figure 1d). These droplets build up a heterogeneous and continuously varying material composite. Novel to this approach, the use of hydrogel-like "support" material mixtures in combination with rigid or flexible "build" materials enables the 3D printer to fabricate custom digital materials that possess relevant properties for the absorption and retention of chemical signals. Further, custom inducer-containing resin formulations (Figure 1e) were developed to enable the direct distribution of both chemical signals and chemical-retentive matrices into the permanent structure of the print (Figure 1f).

To realize a programmed biohybrid function, the 3D-printed object was inoculated with engineered cells (e.g., *Escherichia coli*) that are adhered across the object's surface via a thin, aerosolized hydrogel coating (Figure 1g). The biological behavior of the HLM was mediated by the diffusion of chemical signals through the hydrogel layer, and the capacity of the cells to sense chemical signals predictably and respond in accordance
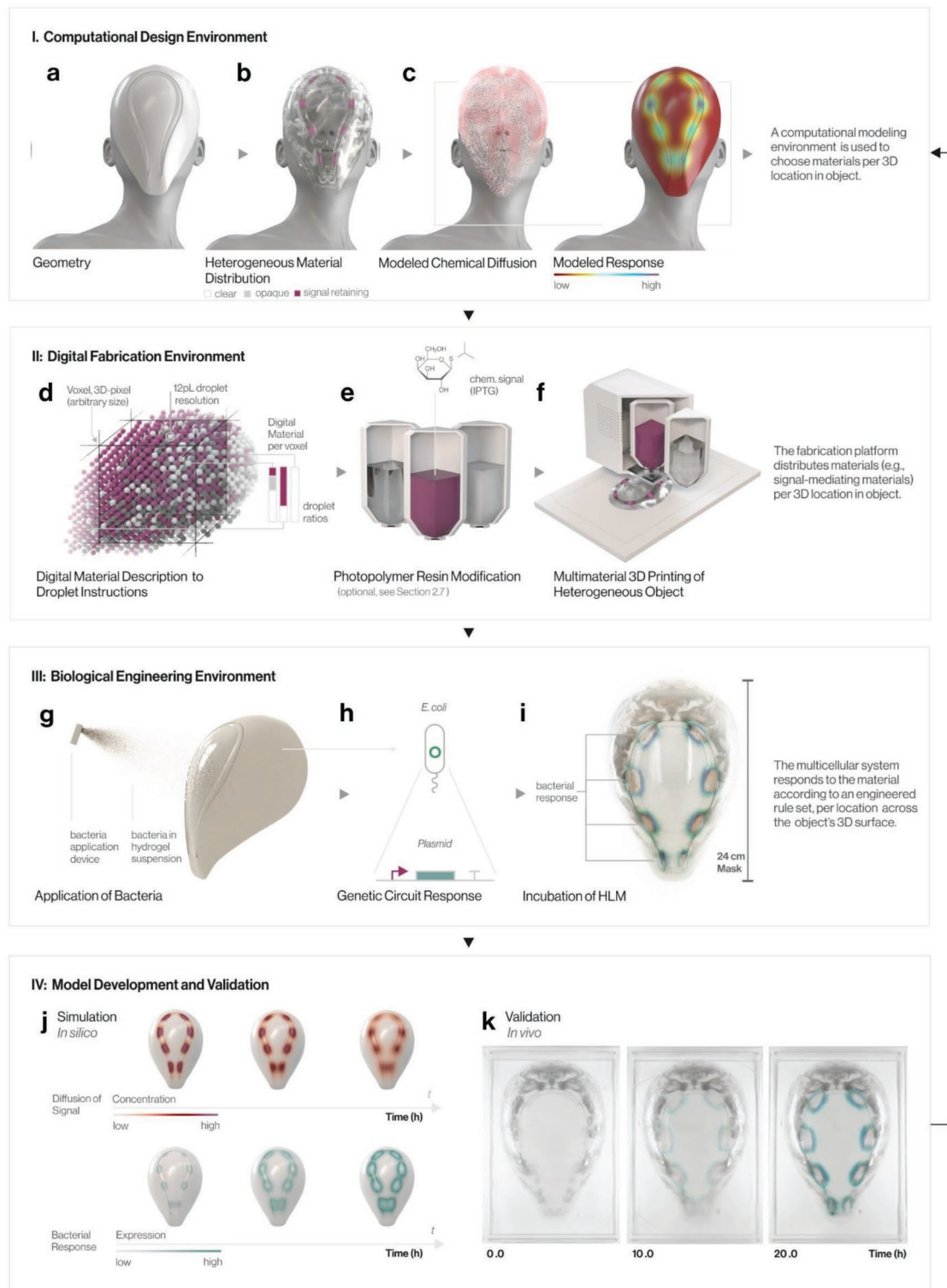
ADVANCED
SCIENCE NEWS
www.advancedsciencenews.com

ADVANCED
FUNCTIONAL
MATERIALS
www.afm-journal.de

Figure 1. An iterative framework for the design and fabrication of hybrid living objects. The framework encompasses components from I) computational design, II) digital fabrication, III) biological engineering, and IV) simulation. a–c) Computational design: a) the computational design process for HLM objects defines surface geometry b) and internal material distributions of the desired object—for instance, a 25 cm custom biohybrid mask, fit to a human face. c) Material distributions specify the placement and concentration of chemical signals throughout the part and can be used in a model of signal diffusion and biological response. d–f) Digital fabrication: d) for production on a multimaterial inkjet-based 3D-printing platform, first, material descriptions in the form of voxels are decoded to droplet deposition instructions for the creation of tunable digital materials, including compositions that enable chemical signal retention. e) With respect to the chemical signal incorporation method (see Section 2.4), custom chemical signaling resins can be developed to enable the platform to deposit signal(s) directly into the 3D-printed architecture, during the printing process.

**ADVANCED
SCIENCE NEWS**

www.advancedsciencenews.com

**ADVANCED
FUNCTIONAL
MATERIALS**

www.afm-journal.de

to a genetically engineered rule set (Figure 1h). Final outputs demonstrated that this methodology may be used to design and fabricate HLMs with predictable and replicable spatiotemporal functions and biological templating (Figure 1i).

Due to the replicability of a digitally controlled biological response, experimental data collected from cell–material interactions aided the development and refinement of a simulation of chemical signal diffusion and engineered genetic response on HLMs (Figure 1j,k). Integrating experimental data into the CAD environment thus yielded an informed design tool for programming interactions between 3D-manufactured materials and engineered bacteria. This modeling tool feeds back into the initial CAD step, thus creating a virtuous cycle for refining predictions of spatially templated biological behavior and function for subsequent HLMs. The following subsections of the "Experimental Section" detail the materials studies and processes leading to the establishment of the HLM fabrication platform.

2.2. Digital-to-Physical Object Description

The Objet Connex500 (Stratasys, Rehovot, Israel) multimaterial inkjet-based 3D printer was the main digital fabrication tool for the HLM framework due to its high resolution, unique control of multiple material jetting, and inherent ability to create complex self-supporting structures.[49] Photopolymeric inkjet-based 3D printers print a wide range of material properties by using a large array of ejection nozzles to deliver droplets of photopolymer resins to targeted positions within a macroscale build space ($40 \times 50 \times 20$ cm), and further blend the loaded materials on the fly to create an expansive range of digital material combinations. The use of a well-established and commercial printer makes the platform presented more tractable and easy to adopt for the production of biohybrids across applications.

To tailor the printer's capabilities for chemical signal printing, the printer was operated using a bitmap-based printing[50] or voxel printing[51] technique. Using a recently developed data-driven material modeling (DDMM) approach,[33,34] a voxel-based digital file of a 3D object was decoded into a set of Z-slices with a slice thickness being set by the native height resolution of the printer (32 µm). For each resin type, the XY-dimension of each Z-slice was represented in as a bitmap file, in which each pixel represented an individually addressable binary command for resin droplet deposition. Unique to HLM fabrication, this approach to material assignment was used to instruct the printer to make new resin combinations for the creation of absorptive materials that immobilize aqueous chemical signals (see Section 2.3). The capacity to deposit consistent droplet volumes

(12 pL) of material at a high level of spatial accuracy was additionally leveraged to precisely distribute chemical signals throughout the build volume of 3D structures (see Section 2.7). This approach allowed for the production of complex 3D geometries with excellent digital controllability over position of absorptive material properties and concentrations of chemical signals.

2.3. Digital Material Discovery for Signal-Releasing and Biocompatible Substrates

The Objet Polyjet system provides a collection of UV-curable acrylate-based polymer resins that range in composition and cured material behavior, and were characterized previously.[50,52–54] In this study, three print resins, two traditional "build materials," rigid VeroClear (RGD810)[55] and flexible Tango (FLX930),[56] and one "support material" (SUP705)[57]— conventionally a sacrificial material used to print overhangs— were used to create a panel of digital material combinations for a series of experiments to evaluate their potential use as bioactive templating materials and viable substrates for living cells.

Wettability and hygroscopic behavior, which are both associated with a polymer's internal chemistry and crosslinking density,[58,59] were used to identify digital material compositions capable of encapsulating and releasing aqueous chemical signal solutions. Wetting behavior was characterized as a contact angle measured with the Sessile drop method,[60] and hygroscopic swelling was measured by change in weight and volume of each cured polymer over a 24 h soak in water (Figure S1, Supporting Information). Polymer mixes containing SUP705 exhibited up to a tenfold decrease in wetting angle and a twofold greater swelling equilibrium by weight than their build material counterparts. These support material- containing formulations were thus well suited for the absorption and release of liquids, and represented candidate digital materials for embedding chemical signal solutions into 3D-printed objects.

To test biocompatibility, printed polymer samples were introduced to early log-phase *E. coli* in liquid culture and incubated for 48 h. A LIVE/DEAD assay performed on the cells and quantified through fluorescence-activated cell sorting (FACS; Figure S2, Supporting Information)[61] verified *E. coli* viability (<50% of population was dead/injured) for all material compositions, but showed better compatibility (<15% of population was dead/injured) for SUP705-build material intermediates than for pure SUP705. These findings suggested that polymer intermediates created by unconventionally blending SUP705 into build materials provided suitable substrates for cell culture, while creating an absorptive matrix to store and release

---

f) The platform outputs a heterogeneous material composite with local control of signal retaining matrices, and/or multiple embedded chemical signals. g–i) Biological engineering: g) bacteria within a hydrogel suspension are applied and immobilized, via a thin aerosolized coating, to the 3D-printed template. h) Engineered cell constructs represent genetic regulatory rule sets, able to respond to cognate diffusing signals at any point across the HLM surface. i) Photograph: the HLM, consisting of living and nonliving components, is incubated for 18–24 h. By hosting and mediating an engineered cellular system, the template material is programmed to generate specified biological response patterning (e.g., color protein expression) at any point across the object surface. j) Simulation: a computational model for the biological response of HLM objects is developed using finite modeling of signal diffusion across 3D geometries and experimental dose–response data per gene construct. k) Validation: time-lapse image of the incubation (37.5 °C, 100% RH) of a 3D-printed wearable HLM mask that gradually yields blue color patterned in prescribed areas, shown at 0, 10, and 20 h, provides one example of platform output in vivo. Image analysis can be used to validate the in silico model of spatial biological response, creating an iterative, self-reinforcing design process for hybrid-living material systems.

ADVANCED
SCIENCE NEWS

www.advancedsciencenews.com

ADVANCED
FUNCTIONAL
MATERIALS

www.afm-journal.de

chemical signals for the purpose of inducing site-specific gene expression. By modulating the concentration of SUP705 in a digital material, the printer platform achieved control of the amount of chemical signal stored per location.

2.4. Chemical Signal Preparation

Chemical signals were introduced to 3D-printed parts in one of two ways. For initial experiments, a method was established that introduced chemical signals after an object was 3D-printed, since SUP705-containing materials absorb aqueous solutions. Objects were 3D-printed and then soaked in a H_2O/dimethyl sulfoxide (DMSO) 50/50 v/v solution containing the specific chemical signal of interest for 12 h. Experiments using isopropyl β-D-1-thiogalactopyranoside (IPTG, 50 mm) and the colorless reagent 5-bromo-chloro-3-indoyl-β-D-galactopyranoside (X-gal, 24 mm) employed the use of *E. coli* cells transformed with pUC19 plasmids. When the 3D-printed object was removed from the bath, only areas containing SUP705 retained the chemical signals. Chemical signals were later incorporated directly into the objects during the printing process using custom resins (see Section 2.7), eliminating the soaking step and allowing for multiple chemicals to be placed simultaneously. In this case, the patterning of SUP705-intermediate materials at the surface of the object was still key to the release profile of chemical signals from the cured structure.

2.5. Cell Cloning

E. coli strains were chosen for the initial HLM platform because they proliferate rapidly, are relatively hardy, and are highly tractable for genetic engineering applications. In this study, these cells represent the agents performing local logic functions in response to the local chemical signal environments programmed into the 3D-printed objects. Figures S3 and S4 (Supporting Information) map the gene constructs engineered to produce the signal-gated visual outputs (colorimetric and fluorescent) used to monitor the spatial and temporal protein expression levels on HLMs. For instance, *E. coli* (K12-derivative, NEB Turbo) with the pUC19 plasmid performed IPTG-gated β-galactosidase (β-gal) expression to catalyze insoluble color production (e.g., blue and magenta) on the surface of HLM objects. Experiments requiring a direct reporter of protein expression level (as opposed to an enzyme–substrate assay) used strains with green and red fluorescent protein (GFP, RFP) outputs. A library of transcriptional regulator constructs for one- and two-input logic functions—including $\overline{IPTG.AHL}$/^{GFP} and IPTG.AHL/^{GFP}, equated to NAND and AND functions, respectively—were utilized for experiments in multisignal pattern generation and computational model development for the HLM platform. Details of these constructs are described in Supplemental Methods in the Supporting Information.

2.6. Bacterial Cell Culture on 3D-Printed Objects

Agar-agarose hydrogels represent a well-characterized, practical choice to adhere cells to the surface of 3D structures, maintain viability of the immobilized cells, and facilitate chemical signal diffusion.[62] This method used a hydrogel composition of 1% agar/1% agarose/25% luria-bertani broth (LB), heated to 100 °C and then cooled to 50 °C for the addition of antibiotics and an overnight culture of cells (final cell concentration $\approx 1 \times 10^7$ colony-forming units (CFUs) mL^{-1}[63]). Using a technique of dispersing cells similar to Sosnowski et al.,[64] the homogenized hydrogel-bacterial slurry was evenly sprayed onto the surface of a 3D-printed object. Importantly, the hydrogel is nontoxic to cells before gelation, and thermal hysteresis properties offer a window of time for cell incorporation into a hydrogel melt before setting at ≈ 35 °C; gelation typically occurred upon contact with the surface of the 3D-printed object. Hydrogel adhesion to the object was facilitated by hydrophilic properties of print materials (Figure S1, Supporting Information). On flexible printed materials and even after deswelling or complete desiccation, the mechanical properties of the hydrogel (i.e., elastic modulus on the order of 100 kPa) helped to prevent delamination.[65] Finally, at 2% w/v total concentration, a 480 Å pore size was anticipated to generate little transport resistance for diffusing solutes ≤ 150 kD.[66]

HLMs with hydrogel coatings were incubated for up to 30 h at 37.5 °C and 100% relative humidity (RH). Microscopy showed successful and characteristic colony growth and metabolic function within gelled suspension (Figure S5, Supporting Information).[67] Thus, the hydrogel surface layer served several purposes including providing an adhesive, nutrient-rich, hydrated matrix for promoting cellular function on HLM surfaces (e.g., proliferation, detection of extracellular signals, and protein expression), and facilitating chemical signal diffusion from within HLMs' printed matrices. For discussion of the hydrogel's long-term stability, see the "Discussion" section.

2.7. Modifications for Chemical Signaling Resins

As a final physical adaptation for facilitating the HLM platform, custom resins were developed to enable multiple chemical signals to be independently controlled by print heads and directly embedded into the 3D-printed objects. To accomplish this, a panel of three chemicals—IPTG, *N*-acyl homoserine lactone (AHL), and Rhamnose (RHA)—and cognate signal-gated GFP-reporting cell constructs were confirmed to have acceptable signal orthogonality on HLMs (Figure S6, Supporting Information), and then were used to assess the chemicals for resin candidacy by investigating their compatibility with print head function and the conservation of their biological function after printing.

Each chemical additive was fully dissolved in H_2O/DMSO (50/50 v/v) before mixing with the SUP705 resin, to ensure that no solid particulates damaged the print head. However, the addition of solvents to resin is known to alter a resin's viscoelastic shear properties, and thus droplet ejection.[68] Hence, a rotational rheometer (Discovery HR-3) was employed to define the upper limit of solvent addition. Using a concentric cylinder geometry, the relative shearing behavior of candidate resin mixtures was measured (Figure S6c, Supporting Information). Solvent mixes of 1% v/v or less exhibited no significant changes ($p < 0.05$) in shear properties in comparison to the original SUP705 resin, and thus defined the tolerance for the addition of solvent in custom resins.

**ADVANCED
SCIENCE NEWS**
www.advancedsciencenews.com

**ADVANCED
FUNCTIONAL
MATERIALS**
www.afm-journal.de

Next, for chemical signal degradation, post-incorporation into resin and exposure to a UV-light dose representative of the printing process were screened. The efficacy of candidate chemical signals embedded in cured resin was evaluated as the level of fluorescent induction from cognate bacterial strains. Figure S6d (Supporting Information) shows that UV-cured IPTG (2.0 m) and AHL (20 µm) resins were still able to generate a robust induction in respective *E. coli* strains (IPTG/^{GFP}, AHL/^{GFP}). However, RHA (2.0 m) failed to elicit a strong biological response from an RHA-inducible strain (RHA/^{GFP}) within the 1% v/v chemical addition limit and was thus eliminated from subsequent investigations. Collectively, this series of validation tests created a methodology to rapidly generate new custom chemical signaling resins that are safe and effective for Objet Polyjet printing. The resin mixtures comprising of IPTG (2.0 m, 0.1–0.05% v/v) and AHL (50 mm, 0.04% v/v) were used for subsequent direct printing experiments.

Collectively, the methods prepared the digitally controllable printing platform to interface with synthetic gene circuits for the goal of a replicable biohybrid fabrication process within user-designed control. In the "Results" section, what can be produced via this approach is explored.

3. Results

The work of developing the HLM platform addressed three major objectives. Primarily, the results demonstrated the feasibility of using digital material descriptions to guide bacterial gene expression across the surface of a 3D-printed object. Prototypes demonstrated that printed material distributions allowed for tunable release of chemical signals, in addition to the ability to generate complex, free-standing, 3D, multimaterial, multifunctional hybrid living objects (Section 3.1). Second, the results showed that augmented resins enabled the 3D printer to pattern multiple chemical signal channels. Using those materials to regulate multi-input synthetic gene constructs, we demonstrated the robustness of the platform to generate spatial patterning based on multiplexed gene expression (Section 3.2). Finally, the results established a computational model to simulate chemical diffusion dynamics and biological response given a volumetric material distribution, thereby providing a predictive design tool for HLM fabrication (Section 3.3).

3.1. Spatiotemporal Control of Gene Expression across 3D-Printed Structures

Initial experiments with the HLM platform aimed to characterize the controllability of spatiotemporal gene induction produced by printed objects. We hypothesized that the platform would enable a replicable response in engineered bacteria across 3D surfaces, including producing an expected result from variables, such as diffusion, that are not within the printer's direct control. To define the relationship between printer-mediated chemical signal placement and cellular response, we printed a set of multimaterial test templates: Vero disks (50 mm diameter, 3 mm height) with 10 mm center regions of incremental digital material compositions (SUP705/RGD810

ratio, 0–1.0, with 0.1 steps), termed "active regions" (**Figure 2**b). Following the HLM fabrication process, disks were soaked in an IPTG/X-Gal bath and incubated with a pUC19 *E. coli* hydrogel layer. Resulting LacZ gene expression patterns (blue) were observed on the objects' surfaces via locally induced *β*-gal activity (Figure 2a).

Results presented in Figure 2c show bacterial response to templates of varied digital materials and plot the relative colorimetric intensity per radial distance from the active region. Importantly, line thickness represents one standard deviation of the average of four experimental replicates, and hence, the consistency in outputs. Gene expression on the HLM objects correlated positively to the ratio of SUP705 within the active region, indicating that bacteria were responding proportionally to the amount of chemical-releasing material in the printed structure. Active regions composed of no SUP705 had negligible expression. Expression patterns were radially symmetrical from the active region, denoting that the hydrogel facilitated even chemical signal and substrate dispersion from the 3D-printed structure. However, at higher SUP705-ratios (>0.7), a ring of decreased expression appeared around the active region (see the "Discussion" section). Importantly, the spatial response of HLM objects, consisting of living cells and multimaterial 3D-printed components, was repeatable and tunable to the SUP705 material ratios defined by the print description.

In Figure 2d, chlorophenol red-*β*-D-galactopyranoside (CPRG) was used in place of X-Gal for another set of HLM test disks to observe the temporal aspects of HLM response. Time-lapse image capture of the incubation of HLMs ($n = 4$) showed a period of CPRG diffusion from the active region (yellow, 0–18 h). At 18 h, the *β*-gal-catalyzed colorimetric conversion of CPRG to chlorophenol red (CPR, magenta) first became visible and continued to intensify and propagate (18–35 h). From these observations, we presume that the rate of signal release does changes over time, and eventually attenuates due to the finite amount of chemical stored. Yet signal release time is relatively well matched to bacterial growth and expression for a robust and consistent final output. These results demonstrated that the spatial and temporal behavior of the HLM templates relied on both the diffusion profile of chemical signal and the response profile of engineered cells, which was used to inform a representative framework for the model for HLM behavior (see Section 3.3).

We next produced HLMs to illustrate digitally driven templating based on reproducible expression behavior. Figure S7 (Supporting Information) shows the bacterial response of HLMs generated from a continuous linear material gradient. The recorded pattern was profiled across ten cross sections and then used to guide the redistribution of digital material in the design of a second HLM template. On the subsequent HLM, an expected oscillating pattern was achieved. Thus, enabled by a reproducible HLM response to digital material, the original template served as a standard on which to base subsequent designs. In Figure S8 (Supporting Information), a resolution template was prepared. While output resolution is reliant on factors outside of printer control (e.g., diffusion and cell sensitivity), a template can qualify the effect that print parameters (e.g., geometry, digital material composition) have on the lower limit of the IPTG/X-gal signal response. On this template, the lower limit of visible response (≥10% relative saturation) was described as a SUP705 surface

**ADVANCED
SCIENCE NEWS**
www.advancedsciencenews.com

**ADVANCED
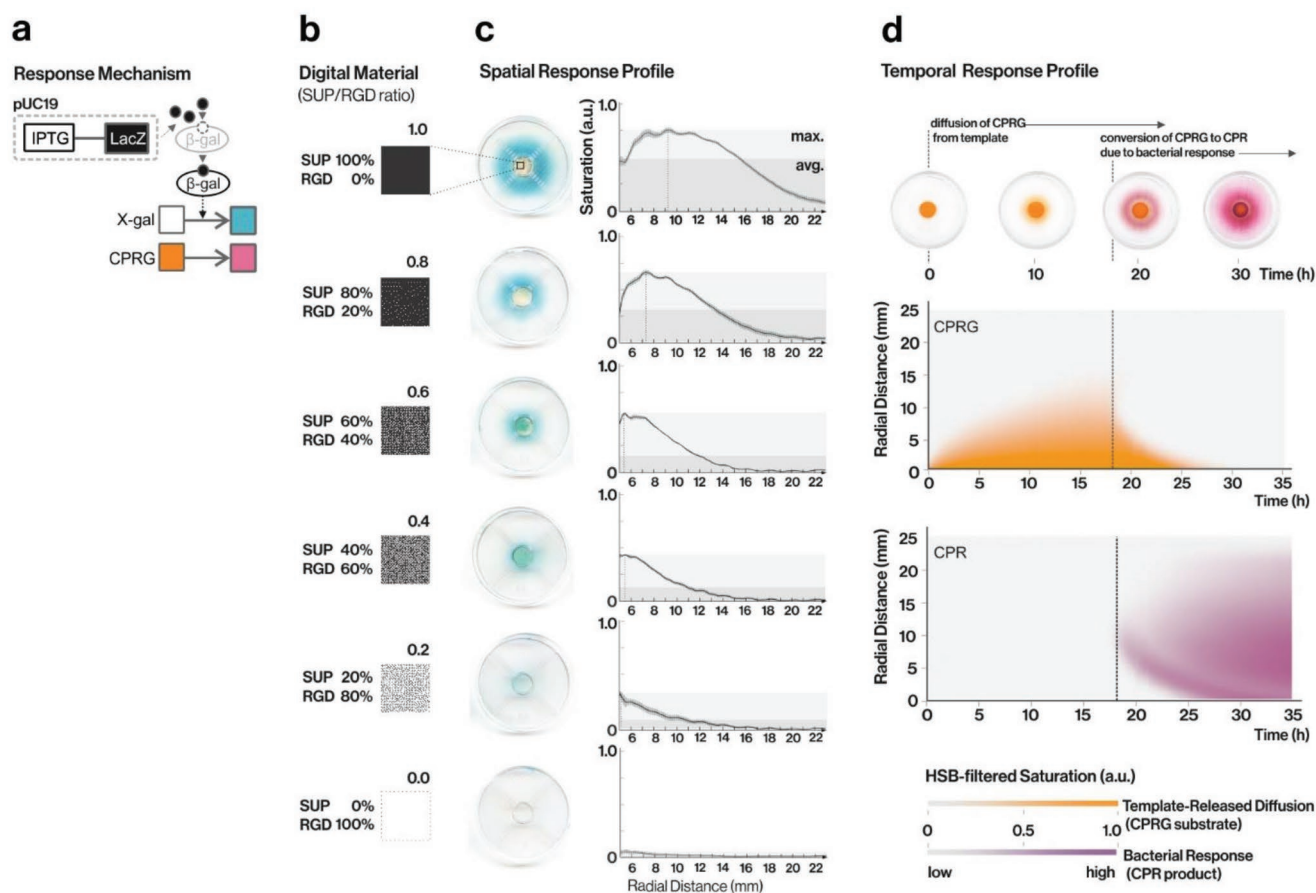FUNCTIONAL
MATERIALS**
www.afm-journal.de

Figure 2. Characterization of chemical signal-retaining digital materials. a) Schematic of the Lac-regulated expression in pUC19 *E. coli* constructs and resulting chromogenic β-gal activity. b) 50 mm diameter RGD810 disk templates contained 10 mm diameter active regions, which consisted of varying SUP705/RGD810 digital materials; the box represents samples of the bitmap droplet instructions, in the form of dither patterns for each blended intermediate (1 pixel = 1 droplet, 600 dpi). c) HLM disks were 3D-printed, soaked in an IPTG-X-gal solution, and coated with a hydrogel suspension of pUC19 cells. After a 30 h incubation, the chromogenic response (blue) derived from β-gal activity was observed. Relative chromogenic saturation (a.u.) is shown as a function of radial distance outward from the edge of the active region (mm), for the average of four replicates of the experiment ($n = 4$). Line thickness represents one standard deviation. The material ratio of SUP705 per template correlates the spatial response of the system. d) The indicator CPRG (yellow) is used as a spatiotemporal visualization of the chemical release profile; β-gal conversion of CPRG to the CPR product (magenta) is used as a visualization of bacterial response. For the average of four replicate experiments run in parallel ($n = 4$), saturation of each color indicator was measured over radial distance from the edge of the active region (mm) and time (h), collected via time-lapse image data.

feature of at least a 24 droplet cross-sectional area (0.08 mm²), or at least a 0.45 SUP705 ratio for any feature above 120 droplet cross-sectional area (0.4 mm²). Importantly, each rule set derived from an observed interaction between the 3D-printed material and a bacteria-signal coupling is accessible via digital parameters afforded to users through the HLM platform.

Finally, the HLM framework was used to produce combinatorial physical property distributions within biohybrid objects, including stiffness and opacity. High-resolution photopolymeric inkjet printing has been shown to generate objects with heterogeneous physical properties widely used in industrial production. Thus, our method enables functional products with augmented biological functionality. **Figure 3** shows biologically and materially patterned HLM objects: optically patterned wearable masks and soft bandage-like patches with programmed bacterial surface activity.

In Figure 3a,b, the masks produced on the HLM platform feature distributions of rigid clear (RGD810), rigid opaque

(RGD835), and chemical signaling materials, for the simultaneous digital control of optical properties (i.e., transparency) and bioactivity (i.e., local colorimetric protein expression). With the mask, we also contrasted the total build envelope (49 × 39 × 19 cm) with the smallest feature size (12 pL, ≈1.2 mm³) to demonstrate the sophistication of internal material distributions and print control across 12 orders of magnitude (Figure 3c). In the production of soft devices, a conformable bandage-like prototype was fabricated using distributions of rigid (RGD810), rubber-like (FLX930), and chemical signaling materials to exhibit site-specific flexibility and bioactivity (Figure 3d). The resulting construct produced a programmed bacterial response across a variable flexible-to-rigid substrate, designed to twist along one axis in a manner that would be applicable to ergonomic support or local conformation to the body (e.g., for biomedical splints, sockets, or bed rests).[69,70]

Overall, the biohybrid artifacts produced illustrate the unique potential of the HLM framework to deploy tunable levels of
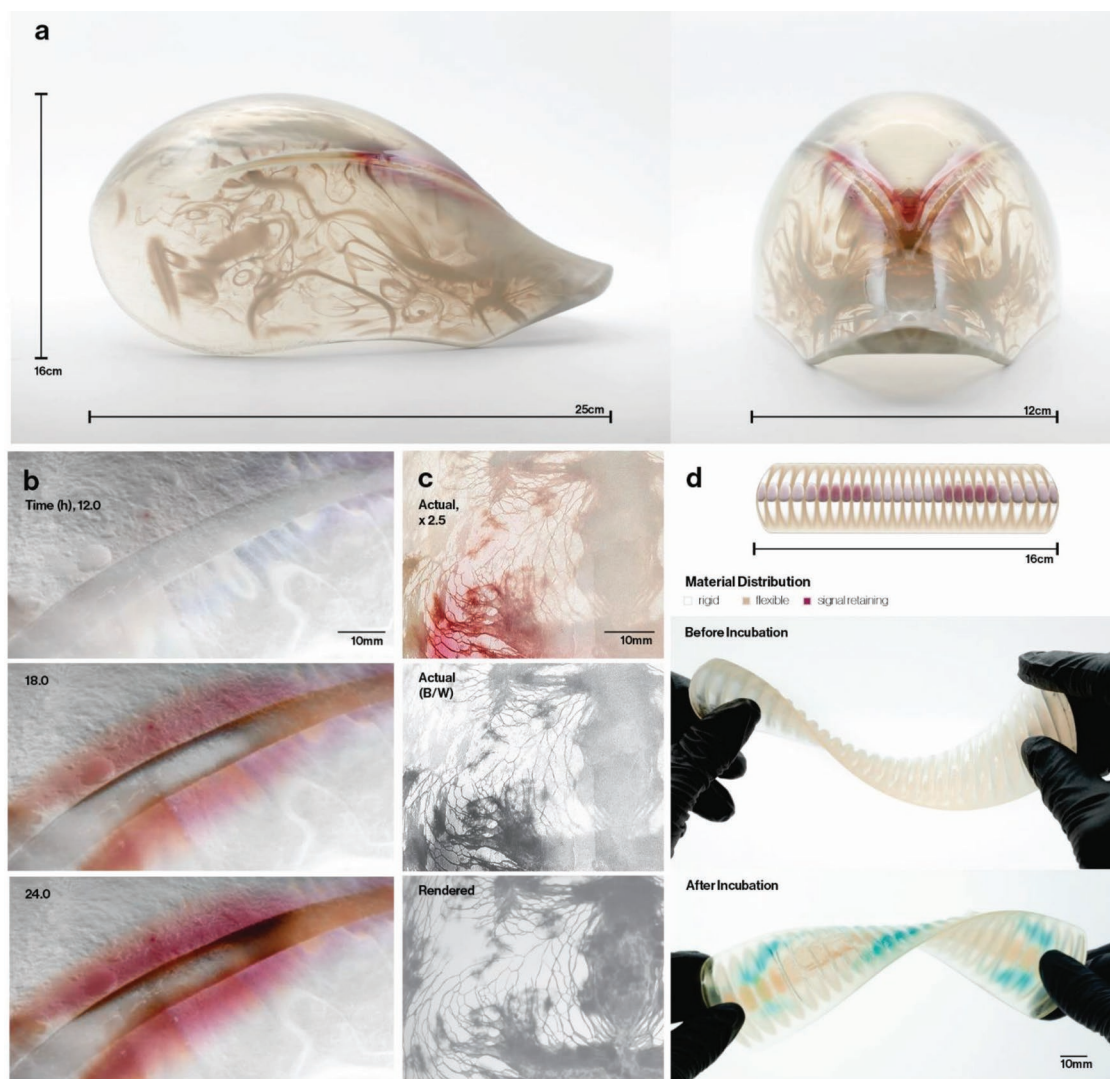
**ADVANCED
SCIENCE NEWS**
www.advancedsciencenews.com

**ADVANCED
FUNCTIONAL
MATERIALS**
www.afm-journal.de

Figure 3. Large-scale HLM device prototypes with graded physical properties. a) A wearable scale object (mask) with designed heterogeneous distributions of opacity and chemical signal concentration demonstrates size and material complexity of the objects achieved through our framework. b) Time-lapse of the mask's surface, showing bacterial response (e.g., chromogenesis) develop according to programmed material distribution during hours incubated (h). c) 2.5× magnified view of a wearable mask surface, showing the sub-millimeter resolution of opaque–transparent internal material distributions and feature size. An image of the actual HLM object (top), converted to a B/W grayscale (middle), and is compared to a computational render of the digital material description (bottom). d) A schematic design of an object with graded material distribution of chemical signal (red to gray) and flexibility (brown to white) (top), and the 3D-printed HLM object before and after incubation, demonstrating templated bacterial response and flexibility (bottom).

bacterial expression, in a site-specific manner, across complex 3D objects. The production of self-supporting HLM objects at the wearable scale, featuring combinatorial physical and chemical signaling properties, served to prototype a diversity of unprecedented hybrid living devices that exhibit biotemplating as well as mechanical or ergonomic functionality.

3.2. Multisignal Channel Control of Synthetic Genes for Pattern Regulation

We further modified the HLM platform to print multichemical environments (e.g., multiplexing), for the objective of

controlling cell systems with multi-input gene regulatory constructs across 3D objects. In synthetic biology, gene-based logic gates are commonly constructed to introduce computation-like, "rational" or synthetically tractable regulatory behavior into cells.[35,36,71] Thus, we hypothesized that using the printer's 3D ink-jetting technology to control multiple chemical signals may allow engineered cells to produce "decision-based" outputs not available to chemical diffusion alone.[72]

IPTG and AHL chemical signal additives were incorporated into the UV-curable photopolymer resins, in a process described in Section 2.7. The chemical signaling resins were loaded into printer cartridges to enable their direct deposition via inkjets at the native resolution of the printer. Hence,
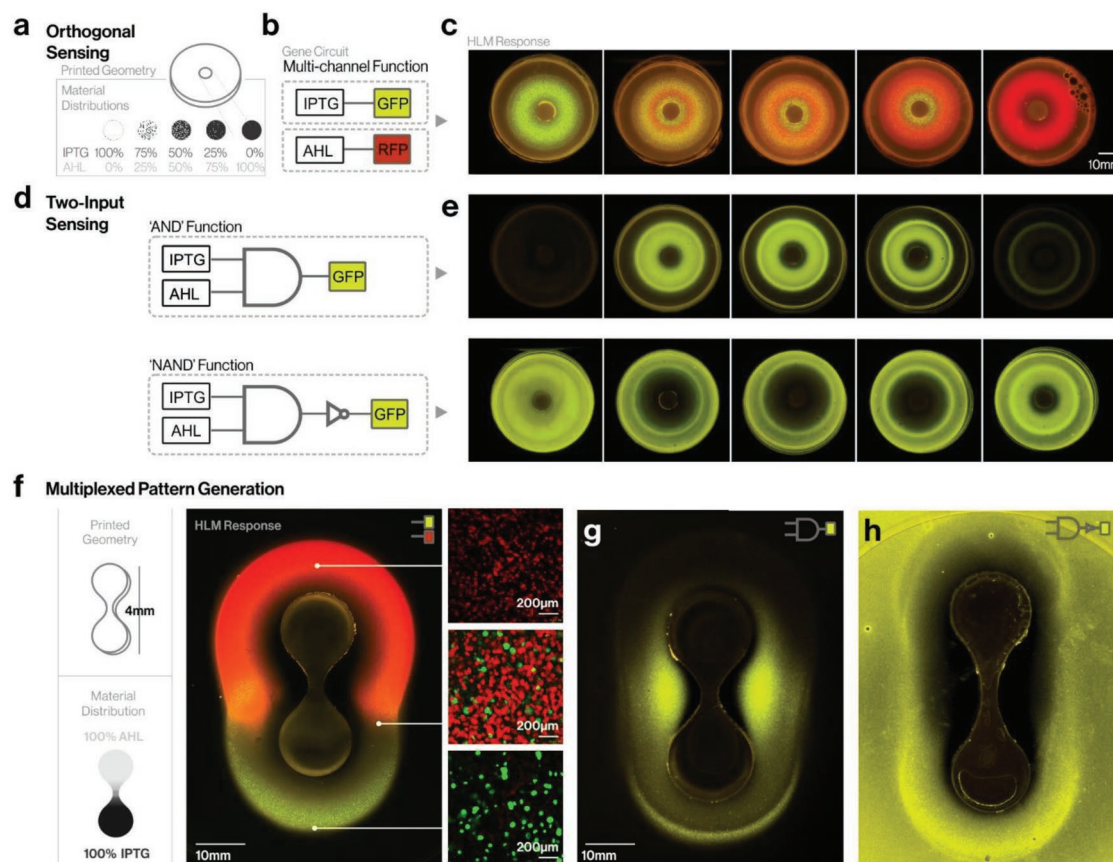
Figure 4. Multiplexed HLM templates generate multisignal patterning and spatial logic. a) The schematic design of disk-shaped templates for testing the 3D printing of multiplexed chemical signaling objects comprised of active regions with intermediate ratios of the two SUP705-based signal resins (IPTG-SUP705/AHL-SUP705 ratio, $n = 4$). b) Engineered gene constructs, IPTG/^{GFP} and AHL/^{RFP}, used to demonstrate orthogonal multioutput patterning. c) Resulting HLM disks demonstrated tunable control and orthogonality between simultaneous protein expression (GFP, RFP) channels. d) Gene constructs engineered for two-input "logic-gates:" an AND function (top), and the inverse, a NAND function (bottom). e) Bacterial AND (top) and NAND (bottom) response on HLM disks, demonstrating that two-input logic functions generate spatial protein expression patterns in relation to regions of two-signal overlap, or lack thereof. f) The schematic design of second template, a two-lobed shape 3D-printed with an internal gradation of two signaling materials (IPTG, AHL) was incubated in contact with an evenly distributed IPTG/^{GFP} and AHL/^{RFP} constructs. The HLM output pattern demonstrated orthogonal regulatory computation for two inputs, per location on the HLM surface, in macro (left), and confirmed by way of confocal fluorescence microscopy (10×) in insets (right). g,h) The two-lobed shaped template was incubated with AND and NAND constructs. The spatial pattern generated demonstrates the relationship of the rule-set (e.g., logic gate) to the HLM template geometry and material distribution.

chemical signal placement was designed and controlled by the CAD environment and soaking the 3D-printed objects post-printing was no longer necessary. The following multiplexed HLM templates were generated for experiments to study multi-input pattern expression: a set of disks with active regions composed of intermediate blends of IPTG- and AHL-signaling material (**Figure 4**a), and a two-lobed shape containing internal gradients of both signaling materials (Figure 4f). Bacterial response patterns were first generated from a mixed population of cells containing genetic circuits IPTG/^{GFP} and AHL/^{RFP} (Figure 4b).

With these amendments to the print system, HLM objects demonstrated simultaneous control over two independently regulated protein outputs (GFP, RFP) across 3D-printed objects (Figure 4c). Using the same cell population, two-lobed HLM objects displayed a multiplexed spatial response made of two independent and overlapping expression patterns, as a result of each chemicals' release profiles (Figure 4f; Figure S9,

Supporting Information). Orthogonal expression of GFP and RFP was confirmed by confocal microscopy of hydrogel samples ($n = 3$) excised from the poles and midsection adjacent to the active region of the HLM.

Further bacterial response patterns were derived from the interaction of materials and cells reporting two-input gene logic. Specifically, gene circuits engineered for AND and NAND regulation of IPTG- and AHL-inputs (Figure 4d) proved responsive to the multiplexed HLM templates. Specifically, patterns generated by AND logic corresponded to HLM areas with threshold concentrations of both signals, and patterns of NAND logic to HLM areas with neither signal (Figure 4e). Spatial output induced by the two-lobed HLM template was observed as a relative fluorescence intensity, with the AND instance showing a fluorescence peak adjacent to the active region's midsection (Figure 4g), indicative of where the two signal release profiles overlap. The NAND instance demonstrated that the inversion of this pattern was also possible (Figure 4h).

Thus, the HLM platform enables multiplexed chemical signaling in 3D-printed objects. The resulting HLMs demonstrated that the digital printing platform can be paired with gene constructs that act as multi-input pattern drivers to generate orthogonal, AND, and NAND computed protein expression patterns on various templates. The allotted control over chemical distributions and engineered cell circuits allows for the systematic design of output patterns.

3.3. Computational Model for HLM Behavior

As a final objective, we created a computational model to predict the biological outcomes of HLM artifacts based on a digital material description in a CAD environment, thereby providing a virtual design tool analogous to other 3D material modeling software.[73,74] Our framework for modeling HLM bacterial response was derived from two underlying processes: the hydrogel-mediated diffusion of chemical signals from a 3D object and the resulting bacterial response. Further, in contrast to existing models,[37,75] the HLM model needed to account for the 3D geometric complexity made possible by the HLM print platform. Thus, we developed a quantitative model, usable in a CAD environment, to account for each of these factors (see Supplemental Methods in the Supporting Information).

First, to simulate hydrogel-facilitated chemical signal diffusion (**Figure 5**a), the model is given a digital print description.

Based upon the volumetric material distribution data, the model derives an initial chemical concentration value per location. Concentration is calculated from the chemical signaling resin composition, or, for soaked templates, the swelling characterization of SUP705-materials (Figure S1, Supporting Information). The transportation of a chemical signal over a regular closed surface $\Gamma \subset \mathbb{R}^3$ was approximated by

$$\partial_t c(x,t) = D\nabla_\Gamma^2 c(x,t) \; \forall x \in \Gamma \text{ and } t > 0 \tag{1}$$

$$c(x,0) = c_0(x) \; \forall x \in \Gamma \tag{2}$$

where ∇_Γ^2 is the surface Laplace–Beltrami operator, $c(\cdot,t): \Gamma \to \mathbb{R}$ is the concentration of a diffused chemical signal, $t \geq 0$ is time, D is the diffusion coefficient, and $c_0: \Gamma \to \mathbb{R}$ is the initial concentration of chemical signal embedded (or stored) in the HLM template. Each chemical signal molecule was assigned a diffusion coefficient D; for example, IPTG in hydrogel was previously experimentally derived[76] to be $D_{IPTG} = 3 \times 10^{-10}$ m^2 s^{-1}. For spatial discretization, the regular surface was assigned a simplicial mesh, and chemical signal concentration was approximated as a piecewise linear function upon this mesh.[77] For temporal discretization of Equation (1), large time steps were essential for fast design iteration and employed an implicit integration scheme.

Second, to simulate bacterial response, the model mapped chemical diffusion profiles to gene expression response
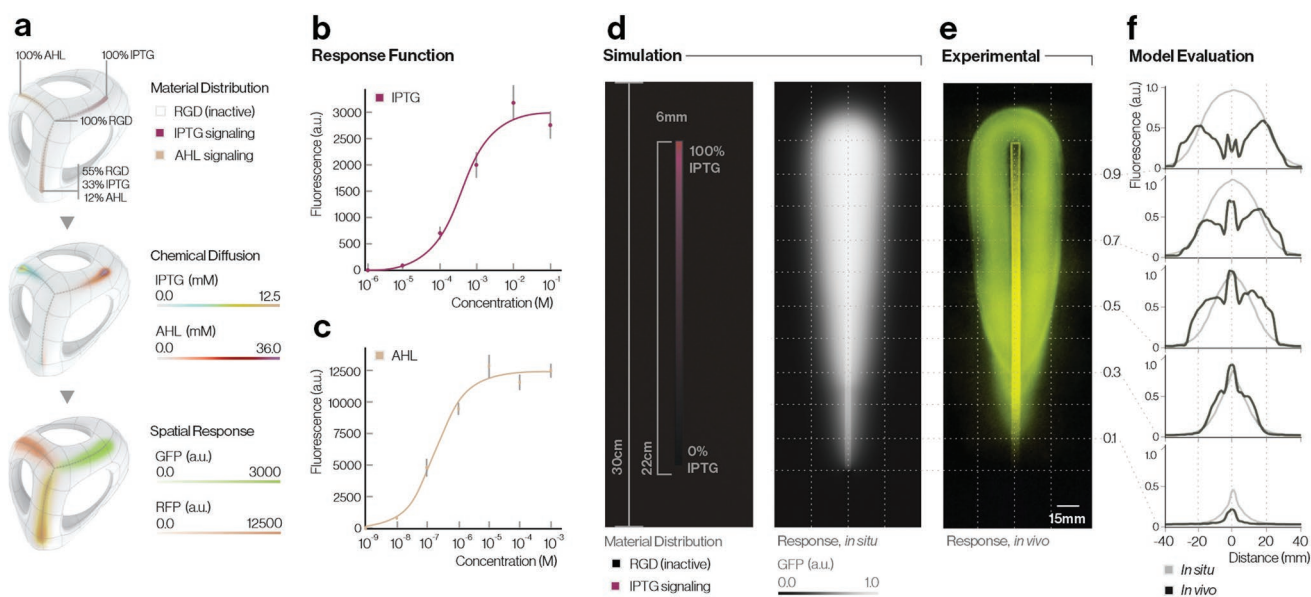

Figure 5. A computational model of HLM-programmed biological response. a) The modeling process to predict HLM outcome, applied to an arbitrary 3D object with multiple signals: first, the material distribution created within the HLM framework is imported (top); the model performs finite analysis of hydrogel-mediated chemical diffusion across the object surface, over time (middle); signal concentration is translated to a spatial response, by way of a defined biological dose–response curve, for the resulting HLM (bottom). b,c) Dose–response curves for IPTG/GFP and AHL/RFP were experimentally obtained through fluorescence measurements (Ex: 485 nm and Em: 528 nm) of cell response to respective inducer concentrations in growth conditions matched to immobilization on HLM object surfaces (24 h). Plot represents the average of four wells per condition (n = 4); error bars represent one standard deviation. The response was fit to a Hill function (plotted line) to define the parameters for the response curves of IPTG/GFP and AHL/RFP, respectively. d) For validation, the computational model is given a material description of a template presenting a linear material gradient of IPTG-SUP705 and RGD810 (left). In silico, the model simulates diffusion of chemical signal concentration on the object over time, and maps a bacterial response, in accordance with the experimental IPTG/GFP response curve of panel (b), for the time point: 24 h (right). e) In vivo, an experimentally generated spatial bacterial response is created by printing the template and incubating with IPTG/GFP for 24 h. f) Comparison of in silico and in vivo outputs, as cross-sectional profiles of bacterial response as a function of relative fluorescent signal (a.u.) at multiple positions along the object.

curves. Figure 5b,c shows experimentally established response curves for IPTG/GFP and AHL/GFP reporter strains. These data were collected in a 96-well plate experiment measuring relative fluorescence readouts of each strain for defined chemical signal concentrations. Fitting the data to a Hill function $h(c) = \dfrac{bc^n}{k^n + c^n}$ we obtained the parameters $b = 4485.93$, $k = 10^{-3}$, $n = 0.95489$ for IPTG, and $b = 45\,837.9$, $k = 4.833 \times 10^{-6}$, $n = 0.877744$ for AHL. However, response curves can also be estimated via a process similar to that in Figure 2c (if fluorescent measurement is not feasible), or from literature or existing gene circuit databases.[78,79]

Figure 5d exhibits the modeled HLM bacterial response at a 24 h time point, and, Figure 5f, the corresponding experimentally prepared 3D-printed template, with an IPTG/GFP strain at 24 h incubation. The simulated response was compared to the experimentally obtained response using relative fluorescent intensity profiles at multiple cross sections across the geometry. The model was most accurate at a 20–40 mm distance to the chemical signal active region. Yet, diminished GFP expression observed in the region closest (>20 mm) to the diffusion source was not accounted for by the model, indicating that there are still factors having a nontrivial impact on HLM expression patterns (see the "Discussion" section).

This simulation can largely predict material-driven signal diffusion and biological responses across 3D surfaces and operate out of the CAD environment used to model the material distributions of HLMs, thus aiding in the design of custom biological outcomes. Comprising of a parametric architecture, the model can accommodate various chemical signals and gene-regulated responses, by inputting different diffusion coefficient and response curve values. As the bioengineering field increasingly adopts strategies for more wide ranging digital control of biological agents, our model provides a repeatable process within user-controlled parameters.

4. Discussion

Existing industrial processes utilize well-characterized materials to produce outcomes that are replicable, scalable, and subject to standardized control. In contrast, a foremost challenge to the advancement of biohybrid materials, and biological materials, in general, is producing consistent outcomes on demand.[80,81] In developing the HLM platform to bridge biohybrid materials to repeatable industrial processes, we observed that reliable biohybrid performance is limited in part by cellular factors (e.g., inconsistent regulatory response) and external factors (e.g., variable environmental conditions). For the initial platform, we addressed consistent cellular behavior by using a highly tractable cell strain, E. coli, and systematically engineered, stable gene circuits. However, we also discuss other model cell chasses that offer compelling lines of inquiry and foreseeable utility. Furthermore, in preventing external factors from disrupting HLM performance, we discuss the efficacy of the materials used in this platform (i.e., hydrogels, photopolymers) and potential future variants.

The HLM platform employed E. coli to capitalize on the broad knowledge base and most recent advancements in the synthetic functionalization of bacterial cells. We demonstrated that enzymatic and fluorescent proteins can be encoded for expression; yet, in the broader context of bioproduction, the HLM platform can be extended to template diverse metabolic outputs, such as functional chemical syntheses across 3D structures (e.g., point-of-use drug production)[1] or material surface treatments (e.g., mineralization or enzymatic digestion).[82] For instance, a biohybrid device with customized and localized production of topical therapeutic agents could help maximize the therapeutic and cost efficiency of treatments, while simultaneously reducing systemic or off-target side effects of drugs.[72,83] Beyond simple constitutive expression systems, synthetic gene circuits can be designed to drive increasingly sophisticated forms of biological computation, thereby having the potential to exhibit new phenomena when distributed across chemical-templated surfaces. For instance, HLMs could enable spatial forms of memory across 3D objects,[84] coordinated dynamic or oscillatory (e.g., quorum) surface expression patterns,[71,85,86] or incorporation of external cues (e.g., physiological signals from a device wearer) into localized decisions.[87,88] Moreover, the union of computational modeling and digital print platform achieved here creates a tractable experimental and simulation space to aid the study of synthetic morphogenesis.[89]

While E. coli provided a proof of concept for the HLM platform, other cell lines may be utilized in future biohybrid research with this platform, thereby providing different functional properties to HLM constructs. For example, candidate cells with less stringent culturing requirements, such as Bacillus subtilis[90,91] or insect cells,[92,93] have the potential to provide known properties (e.g., desiccation resistance and actuation). Advantageously, the modular nature of the HLM framework permits the components—both hydrogel and cell strain—to be interchanged in a straightforward fashion without impacting the print regime. Thus, it is feasible for other cell types to be integrated, and a subject of future investigation to study how other cell types respond to digitally controlled diffusive chemical signals or 3D surfaces on this platform.

Regarding external factors impacting the replicability of biohybrid performance, the integrity of the hydrogel was essential for reliable HLM outcomes. HLM activity, with respect to signal diffusion and cell growth, occurred over an 18–35 h period at 100% RH (Figure 2d). When removed from a high-humidity environment, the hydrogel experienced water loss, which interfered with signal diffusivity and cell function. However, hydrogels did adhere to surfaces throughout desiccation, and all stable compounds previously produced (e.g., pigments) would remain laminated to the 3D object's surface once the hydrogel dried. Thus, one can choose from applications intended to have active cell function (an "active-life" of ≈24 h)[44,45] or processes that allow signals and cells to desiccate once the intended surface properties are obtained. Future work may leverage recent advancements in natural and synthetic hydrogels to tune the timeframe of HLM activity, and create more robust, desiccation-resilient constructs.[75,94] Additionally, in consideration of device age, ongoing observations of the IPTG and AHL signaling materials developed for the HLM platform show promise of a considerable ambient shelf life after 200 days (Figure S10, Supporting Information), indicating that HLMs can be digitally

fabricated and stored prior to being "activated" by the addition of hydrogel.

Finally, in some instances, our platform experienced unexpected outputs due to photopolymeric compositions. Specifically, surface regions adjacent to some digital materials (SUP705/RGD810 ratios > 0.7 in Figures 2c, 4c, and 5e) exhibited diminished protein expression—a possible artifact of cell interaction with a material composition that was later demonstrated to lower the pH when exposed to aqueous environments. This effect was not represented by our computational model, yet could be incorporated into future models or design considerations.

5. Conclusion

In conclusion, the HLM fabrication platform provides a new technology centered on bridging computational design, material fabrication, and synthetic biology to control gene expression patterns across the surface of geometrically complex, mechanically robust, multimaterial 3D structures. Specifically, our process modifies the digital commands and material compositions of a 3D-printing platform to fabricate structured photopolymers that can retain precise spatial distributions of chemical regulatory signals within their cured architectures. Subsequently, our method immobilizes engineered *E. coli* on the surface of these objects, to facilitate designed interactions between engineered gene constructs and chemical signaling profiles. Thus, the HLMs presented herein are designed to produce programmed gene-regulated responses across the surface of 3D objects in repeatable and predictable ways.

In contribution to the field of biohybrid materials, our platform demonstrates self-supporting HLM constructions of up to half a meter in length, with freeform shape generation, and the incorporation of site-specific mechanical and optical properties. Because engineered bacterial response was defined in terms of a digital print description, the platform achieved a programmable methodology for producing controlled spatial interactions between 3D-printed digital materials and genetic regulatory circuits. Thus, our platform generated objects with various protein expression patterns from single-input gene circuits and—with the development of multiplexed chemical signal printing—multi-input logic constructs (e.g., AND and NAND regulatory operations). Furthermore, we linked the design-to-output workflow for HLMs by integrating a computational model of signal diffusion and bacterial response across 3D surfaces into a CAD environment. The HLM fabrication platform's capacity to simultaneously direct complex 3D structures, bacterial functions, and material property distributions enables unprecedented control of functional outputs. This work thus advances biohybrid materials toward applications ranging from wearable therapeutics or monitoring devices to customizable consumer products.[95–97]

Supporting Information

Supporting Information is available from the Wiley Online Library or from the author.

Conflict of Interest

The authors declare no conflict of interest.

[1] M. J. Smanski, H. Zhou, J. Claesen, B. Shen, M. A. Fischbach, C. A. Voigt, *Nat. Rev. Microbiol.* **2016**, *14*, 135.
[2] D. Jullesson, F. David, B. Pfleger, J. Nielsen, *Biotechnol. Adv.* **2015**, *33*, 1395.
[3] V. Libis, B. Delépine, J. L. Faulon, *Curr. Opin. Microbiol.* **2016**, *33*, 105.
[4] Z. Ma, F. E. Jacobsen, D. P. Giedroc, *Chem. Rev.* **2009**, *109*, 4644.
[5] P. Q. Nguyen, N. M. D. Courchesne, A. Duraj-Thatte, P. Praveschotinunt, N. S. Joshi, *Adv. Mater.* **2018**, *30*, 1704847.
[6] M. Haneef, L. Ceseracciu, C. Canale, I. S. Bayer, J. A. Heredia-Guerrero, A. Athanassiou, *Sci. Rep.* **2017**, *7*, 41292.
[7] L. Valentini, S. Bittolo Bon, S. Signetti, N. M. Pugno, *ACS Appl. Mater. Interfaces* **2016**, *8*, 7607.
[8] F. Moser, M. Trautz, A.-L. Beger, M. Löwer, G. Jacobs, F. Hillringhaus, A. Wormit, B. Usadel, J. Reimer, *Hamburg Symposium: Materials for Spatial Structures,* (Ed: C. Gantes), IASS **2017**, pp. 1–7.
[9] L. C. Gerber, F. M. Koehler, R. N. Grass, W. J. Stark, *Proc. Natl. Acad. Sci. USA* **2012**, *109*, 90.
[10] Y. Liu, M. H. Rafailovich, R. Malal, D. Cohn, D. Chidambaram, *Proc. Natl. Acad. Sci. USA* **2009**, *106*, 14201.
[11] M. Akbari, A. Tamayol, V. Laforte, N. Annabi, A. H. Najafabadi, A. Khademhosseini, D. Juncker, *Adv. Funct. Mater.* **2014**, *24*, 4060.
[12] S. Xie, S. Tai, H. Song, X. Luo, H. Zhang, X. Li, *J. Mater. Chem. B* **2016**, *4*, 6820.
[13] R. Raman, C. Cvetkovic, S. G. M. Uzel, R. J. Platt, P. Sengupta, R. D. Kamm, R. Bashir, *Proc. Natl. Acad. Sci. USA* **2016**, *113*, 3497.
[14] J. Bastos-Arrieta, A. Revilla-Guarinos, W. E. Uspal, J. Simmchen, *Front. Robot. AI* **2018**, *5*, 97.
[15] L. Ricotti, B. Trimmer, A. W. Feinberg, R. Raman, K. K. Parker, R. Bashir, M. Sitti, S. Martel, P. Dario, A. Menciassi, *Sci. Rob.* **2017**, *2*, eaaq0495.
[16] J. C. Nawroth, H. Lee, A. W. Feinberg, C. M. Ripplinger, M. L. McCain, A. Grosberg, J. O. Dabiri, K. K. Parker, *Nat. Biotechnol.* **2012**, *30*, 792.

ADVANCED
SCIENCE NEWS
www.advancedsciencenews.com

ADVANCED
FUNCTIONAL
MATERIALS
www.afm-journal.de

[17] S. Moon, I. L. Fritz, Z. S. Singer, T. Danino, *3D Print. Addit. Manuf.* **2016**, *3*, 195.

[18] A. L. Rutz, K. E. Hyland, A. E. Jakus, W. R. Burghardt, R. N. Shah, *Adv. Mater.* **2015**, *27*, 1607.

[19] R. G. Wylie, S. Ahsan, Y. Aizawa, K. L. Maxwell, C. M. Morshead, M. S. Shoichet, *Nat. Mater.* **2011**, *10*, 799.

[20] T. Lu, Y. Li, T. Chen, *Int. J. Nanomed.* **2013**, *8*, 337.

[21] S. A. L. de Koster, R. M. Mors, H. W. Nugteren, H. M. Jonkers, G. M. H. Meesters, J. R. Van Ommen, *Proc. Eng.* **2015**, *102*, 475.

[22] A. Y. Chen, Z. Deng, A. N. Billings, U. O. S. Seker, M. Y. Lu, R. J. Citorik, B. Zakeri, T. K. Lu, *Nat. Mater.* **2014**, *13*, 515.

[23] M. Florea, H. Hagemann, G. Santosa, J. Abbott, C. N. Micklem, X. Spencer-Milnes, L. de Arroyo Garcia, D. Paschou, C. Lazenbatt, D. Kong, H. Chughtai, K. Jensen, P. S. Freemont, R. Kitney, B. Reeve, T. Ellis, *Proc. Natl. Acad. Sci. USA* **2016**, *113*, E3431.

[24] M. Mukherjee, Y. Hu, C. H. Tan, S. A. Rice, B. Cao, *Sci. Adv.* **2018**, *4*, eaau1459.

[25] M. Schaffner, P. A. Rühs, F. Coulter, S. Kilcher, A. R. Studart, *Sci. Adv.* **2017**, *3*, eaao6804.

[26] X. Liu, H. Yuk, S. Lin, G. A. Parada, T.-C. Tang, E. Tham, C. de la Fuente-Nunez, T. K. Lu, X. Zhao, *Adv. Mater.* **2018**, *30*, 1704821.

[27] B. A. E. Lehner, D. T. Schmieden, A. S. Meyer, *ACS Synth. Biol.* **2017**, *6*, 1124.

[28] S. V. Murphy, A. Atala, *Nat. Biotechnol.* **2014**, *32*, 773.

[29] F. Moser, E. Tham, L. M. González, T. K. Lu, C. A. Voigt, *Adv. Funct. Mater.* **2019**, *29*, 1901788.

[30] A. Levskaya, A. A. Chevalier, J. J. Tabor, Z. B. Simpson, L. A. Lavery, M. Levy, E. A. Davidson, A. Scouras, A. D. Ellington, E. M. Marcotte, C. A. Voigt, *Nature* **2005**, *438*, 441.

[31] D. J. Cohen, R. C. Morfino, M. M. Maharbiz, W.-S. Chen, J. Axelrod, *PLoS One* **2009**, *4*, e7086.

[32] J. J. Tabor, H. M. Salis, Z. B. Simpson, A. A. Chevalier, A. Levskaya, E. M. Marcotte, C. A. Voigt, A. D. Ellington, *Cell* **2009**, *137*, 1272.

[33] C. Bader, D. Kolb, J. C. Weaver, S. Sharma, A. Hosny, J. Costa, N. Oxman, *Sci. Adv.* **2018**, *4*, eaas8652.

[34] C. Bader, D. Kolb, J. C. Weaver, N. Oxman, *3D Print. Addit. Manuf.* **2016**, *3*, 71.

[35] A. Tamsir, J. J. Tabor, C. A. Voigt, *Nature* **2011**, *469*, 212.

[36] S. Basu, Y. Gerchman, C. H. Collins, F. H. Arnold, R. Weiss, *Nature* **2005**, *434*, 1130.

[37] M. Weitz, A. Mückl, K. Kapsner, R. Berg, A. Meyer, F. C. Simmel, *J. Am. Chem. Soc.* **2014**, *136*, 72.

[38] R. Suntivich, I. Drachuk, R. Calabrese, D. L. Kaplan, V. V. Tsukruk, *Biomacromolecules* **2014**, *15*, 1428.

[39] P. Chen, S. Wang, F. Inci, S. Güven, S. Tasoglu, U. Demirci, in *Gels Handbook* (Eds: L. Kang, S. Majd), World Scientific, Singapore **2016**, p. 327.

[40] A. Goyanes, U. Det-Amornrat, J. Wang, A. W. Basit, S. Gaisford, *J. Controlled Release* **2016**, *234*, 41.

[41] M. Alary, J.-J. Liu, E. Lunde, B. Patel, (Johnson & Johnson Consumer Inc.), *US 2018 0206616 A1*, **2018**.

[42] X. G. Cheng, J. J. Yoo, R. G. Hale, *Regener. Med.* **2014**, *9*, 245.

[43] Y. Wei, Y. Wang, M. Zhang, G. Yan, S. Wu, W. Liu, G. Ji, C. W. P. Li-Tsang, *Burns* **2018**, *44*, 453.

[44] L. C. Gerber, F. M. Koehler, R. N. Grass, W. J. Stark, *Angew. Chem., Int. Ed.* **2012**, *51*, 11293.

[45] M. Kurečič, T. Rijavec, S. Hribernik, A. Lapanje, K. S. Kleinschek, U. Maver, *Nanomedicine* **2018**, *13*, 1583.

[46] A. M. Vargason, A. C. Anselmo, *Bioeng. Transl. Med.* **2018**, *3*, 124.

[47] S. Sankaran, J. Becker, C. Wittmann, A. del Campo, *Small* **2019**, *15*, 1804717.

[48] J.-Y. Lee, J. An, C. K. Chua, *Appl. Mater. Today* **2017**, *7*, 120.

[49] B. Bhushan, M. Caspers, *Microsyst. Technol.* **2017**, *23*, 1117.

[50] C. Bader, W. G. Patrick, D. Kolb, S. G. Hays, S. Keating, S. Sharma, D. Dikovsky, B. Belocon, J. C. Weaver, P. A. Silver, N. Oxman, *3D Print. Addit. Manuf.* **2016**, *3*, 79.

[51] E. L. Doubrovski, E. Y. Tsai, D. Dikovsky, J. M. P. Geraedts, H. Herr, N. Oxman, *Comput. Des.* **2015**, *60*, 3.

[52] Stratasys, Ltd., *Digital Materials Data Sheet*, **2017**, https://www.stratasys.com/-/media/files/material-spec-sheets/mss_pj_digitalmaterialsdatasheet_0617a.pdf, (accessed: December 2019).

[53] K. K. Reichl, D. J. Inman, in *Topics in Modal Analysis and Testing, Vol. 10, Proc. of the 34th IMAC, A Conf. and Exposition on Structural Dynamics* (Ed: M. Mains), Springer, Cham **2016**, p. 191.

[54] J. Mańkowski, J. Lipnicki, *Int. J. Appl. Mech. Eng.* **2017**, *22*, 601.

[55] Stratasys Ltd., *VEROCLEAR RGD810 Safety Data Sheet*, **2019**, https://www.stratasys.com/-/media/B827AE347C0D482FB167F0008D837277.pdf, (accessed: December 2019).

[56] Stratasys Ltd., *OBJET TANGOPLUS FLX930 Safety Data Sheet*, **2019**, https://www.stratasys.com/-/media/E7CB2C-4C1D734A47A78C5909647BB925.pdf, (accessed: December 2019).

[57] Stratasys Ltd., *OBJET SUPPORT SUP705 Safety Data Sheet*, **2019**, https://www.stratasys.com/-/media/03F0FFF15CDE4A4F8E533FBDBB05C069.pdf, (accessed: December 2019).

[58] K.-J. Kim, S.-B. Lee, N. W. Han, *Polym. J.* **1993**, *25*, 1295.

[59] Y. Wu, S. Joseph, N. R. Aluru, *J. Phys. Chem. B* **2009**, *113*, 3512.

[60] Y. Yuan, T. R. Lee, Contact Angle and Wetting Properties (Eds: G. Bracco, B. Holst), *Surface Science Techniques Springer Series*, Vol. *51*, Springer, Berlin **2013**, p. 3.

[61] M. Berney, F. Hammes, F. Bosshard, H.-U. Weilenmann, T. Egli, *Appl. Environ. Microbiol.* **2007**, *73*, 3283.

[62] E. M. Ahmed, *J. Adv. Res.* **2015**, *6*, 105.

[63] G. Sezonov, D. Joseleau-Petit, R. D'Ari, *J. Bacteriol.* **2007**, *189*, 8746.

[64] T. R. Sosnowski, A. Kurowska, B. Butruk, K. Jabłczyńska, *Chem. Eng. Trans.* **2013**, *32*, 2257.

[65] V. Normand, D. L. Lootens, E. Amici, K. P. Plucknett, P. Aymard, *Biomacromolecules* **2000**, *1*, 730.

[66] R. H. Li, D. H. Altreuter, F. T. Gentile, *Biotechnol. Bioeng.* **1996**, *50*, 365.

[67] K. Boons, E. Noriega, R. Van den Broeck, C. C. David, J. Hofkens, J. F. Van Impe, *Appl. Environ. Microbiol.* **2014**, *80*, 5330.

[68] B.-J. de Gans, P. C. Duineveld, U. S. Schubert, *Adv. Mater.* **2004**, *16*, 203.

[69] D. M. Sengeh, H. Herr, *JPO J. Prosthet. Orthotics* **2013**, *25*, 129.

[70] A. M. Paterson, R. Bibb, R. I. Campbell, G. Bingham, *Rapid Prototyping J.* **2015**, *21*, 230.

[71] F. Moser, A. Espah Borujeni, A. N. Ghodasara, E. Cameron, Y. Park, C. A. Voigt, *Mol. Syst. Biol.* **2018**, *14*, e8605.

[72] T. Ozdemir, A. J. H. Fedorec, T. Danino, C. P. Barnes,. *Cell Syst.* **2018**, *7*, 5.

[73] W. Regli, J. Rossignac, V. Shapiro, V. Srinivasan, *CAD Comput. Aided Des* **2016**, *77*, 73.

[74] M. M. Francois, A. Sun, W. E. King, N. J. Henson, D. Tourret, C. A. Bronkhorst, N. N. Carlson, C. K. Newman, T. Haut, J. Bakosi, J. W. Gibbs, V. Livescu, S. A. Vander Wiel, A. J. Clarke, M. W. Schraad, T. Blacker, H. Lim, T. Rodgers, S. Owen, F. Abdeljawad, J. Madison, A. T. Anderson, J. L. Fattebert, R. M. Ferencz, N. E. Hodge, S. A. Khairallah, O. Walton, *Curr. Opin. Solid State Mater. Sci.* **2017**, *21*, 198.

[75] X. Liu, T.-C. Tang, E. Tham, H. Yuk, S. Lin, T. K. Lu, X. Zhao, *Proc. Natl. Acad. Sci. USA* **2017**, *114*, 2200.

[76] S. Lin, H. Yuk, T. Zhang, G. A. Parada, H. Koo, C. Yu, X. Zhao, *Adv. Mater.* **2016**, *28*, 4497.

[77] M. Botsch, L. Kobbelt, M. Pauly, P. Alliez, B. Lévy, *Polygon Mesh Processing*, (Ed: A. K. Peters), CRC Press, New York, NY **2010**.

[78] A. J. Meyer, T. H. Segall-Shapiro, E. Glassey, J. Zhang, C. A. Voigt, *Nat. Chem. Biol.* **2019**, *15*, 196.

[79] A. A. K. Nielsen, B. S. Der, J. Shin, P. Vaidyanathan, V. Paralanov, E. A. Strychalski, D. Ross, D. Densmore, C. A. Voigt, *Science* **2016**, *352*, aac7341.

[80] P. F. Costa, *Trends Biotechnol.* **2019**, *37*, 1032.

[81] H. Cui, M. Nowicki, J. P. Fisher, L. G. Zhang, *Adv. Healthcare Mater.* **2017**, *6*, 1601118.

[82] S. Douglas, T. J. Beveridge, *FEMS Microbiol. Ecol.* **1998**, *26*, 79.

[83] A. K. Ferreira, L. I. Mambelli, S. Y. Pillai, *Best Pract. Res., Clin. Gastroenterol.* **2017**, *31*, 693.

[84] N. Roquet, A. P. Soleimany, A. C. Ferris, S. Aaronson, T. K. Lu, *Science* **2016**, *353*, aad8559.

[85] O. Mondragón-Palomino, T. Danino, J. Selimkhanov, L. Tsimring, J. Hasty, *Science* **2011**, *333*, 1315.

[86] M. O. Din, T. Danino, A. Prindle, M. Skalak, J. Selimkhanov, K. Allen, E. Julio, E. Atolia, L. S. Tsimring, S. N. Bhatia, J. Hasty, *Nature* **2016**, *536*, 81.

[87] T. S. Moon, C. Lou, A. Tamsir, B. C. Stanton, C. A. Voigt, *Nature* **2012**, *491*, 249.

[88] D. T. Riglar, T. W. Giessen, M. Baym, S. J. Kerns, M. J. Niederhuber, R. T. Bronson, J. W. Kotula, G. K. Gerber, J. C. Way, P. A. Silver, *Nat. Biotechnol.* **2017**, *35*, 653.

[89] B. P. Teague, P. Guye, R. Weiss, *Cold Spring Harbor Perspect. Biol.* **2016**, *8*, a023929.

[90] L. M. González, N. Mukhitov, C. A. Voigt, *Nat. Chem. Biol.* **2019**, https://doi.org/10.1038/s41589-019-0412-5.

[91] J. Huang, S. Liu, C. Zhang, X. Wang, J. Pu, F. Ba, S. Xue, H. Ye, T. Zhao, K. Li, Y. Wang, J. Zhang, L. Wang, C. Fan, T. K. Lu, C. Zhong, *Nat. Chem. Biol.* **2019**, *15*, 34.

[92] N. R. Rubio, K. D. Fish, B. A. Trimmer, D. L. Kaplan, *ACS Biomater. Sci. Eng.* **2019**, *5*, 1071.

[93] A. L. Baryshyan, L. J. Domigan, B. Hunt, B. A. Trimmer, D. L. Kaplan, *RSC Adv.* **2014**, *4*, 39962.

[94] H. Yuk, T. Zhang, G. A. Parada, X. Liu, X. Zhao, *Nat. Commun.* **2016**, *7*, 12028.

[95] Y.-F. Zhang, N. Zhang, H. Hingorani, N. Ding, D. Wang, C. Yuan, B. Zhang, G. Gu, Q. Ge, *Adv. Funct. Mater.* **2019**, *29*, 1806698.

[96] A. Nuseir, M. M. Hatamleh, A. Alnazzawi, M. Al-Rabab'ah, B. Kamel, E. Jaradat, *J. Prosthodontics* **2019**, *28*, 10.

[97] J. Holländer, N. Genina, H. Jukarainen, M. Khajeheian, A. Rosling, E. Mäkilä, N. Sandler, *J. Pharm. Sci.* **2016**, *105*, 2665.